

SSL-DG: Rethinking and Fusing Semi-supervised Learning and Domain Generalization in Medical Image Segmentation

Zanting Ye¹

¹The School of Computer Science and Artificial Intelligence, Changzhou University

Abstract

Deep learning-based medical image segmentation is an essential yet challenging task in clinical practice, which arises from restricted access to annotated data coupled with the occurrence of domain shifts. Previous attempts have focused on isolated solutions, while disregarding their interconnectedness. In this paper, we rethink the relationship between semi-supervised learning (SSL) and domain generalization (DG), which are the cutting-edge approaches to address the annotated data-driven constraints and the domain shift issues. Inspired by class-level representation, we show that unseen target data can be represented by a linear combination of source data, which can be achieved by simple data augmentation. The augmented data enrich domain distributions while having semantic consistency, aligning with the principles of consistency-based SSL. Accordingly, we propose SSL-DG, fusing DG and SSL, to achieve cross-domain generalization with limited annotations. Specifically, the global and focal region augmentation, together with an augmentation scale-balancing mechanism, are used to construct a mask-based domain diffusion augmentation module to significantly enrich domain diversity. In order to obtain consistent predictions for the same source data in different networks, we use uncertainty estimation and a deep mutual learning strategy to enforce the consistent constraint. Extensive experiments including ablation studies are designed to validate the proposed SSL-DG. The results demonstrate that our SSL-DG significantly outperforms state-of-the-art solutions in two challenging DG tasks with limited annotations. Code is available at <https://github.com/yezanting/SSL-DG>.

Introduction

Deep learning-based medical image segmentation [1, 2, 13], a fundamental and critical step in computer-aided diagnosis systems, enhance diagnosis efficiency [4, 5]. Recent evidence suggested that its performance comparable to human experts in certain fields [6, 7, 20, 15]. However, most approaches heavily rely on annotated data, posing challenges due to medical data’s sensitive nature, limited shareability, and high costs for pixel/voxel-level annotations [8, 19]. Furthermore, domain shift is quite common among medical image datasets, raising additional challenging for the generalization performance of models. These constraints hinder the

broader adoption of deep learning in medical image segmentation field.

Numerous studies have been made to reduce the dependency on annotated data. A prominent approach is self-supervised learning [9]. While beneficial for natural images, self-supervised learning’s challenge in medical images lies in their complex semantic correlations. By integrating limited annotated data and vast unannotated data, SSL eases the annotators’ workload, guiding models construct decision levels. SSL chiefly focuses on effectively supervising unannotated data [8]. Related researches have primarily bifurcated into two branches: (1) Pseudo-label-based SSL [10]. Here, annotated data is used for initial network training. As the model iterates, it produces refined pseudo-labels from unannotated data for continuous model updates. (2) Consistency-based SSL [11, 12]: These methods employ outputs’ consistency for an unannotated image under different perturbations (e.g., horizontal flip, alterations in contrast and brightness) to update model. Unlike pseudo-label-based SSL, which requires multiple thresholds to counteract the impact of erroneous pseudo-labels, consistency-based SSL present a more stable performance.

In addition to its advantage in feature learning for unannotated data, consistency-based SSL has great potential for domain invariance learning, which is the key to solve domain shift problem. Few researches have, however, been made in this area. Our study, depicted in Fig. 1, delves into the relationship between consistency-based SSL and DG from both a data and a model standpoint, and pioneeringly report SSL-DG, a SSL medical image segmentation framework with cross-modality ability. By looking into the consistency-based SSL and DG, two notable discoveries have been made: (1) Both methods prioritize data augmentation in data processing step. The distinction lies in the fact that the former emphasis on constructing supervised learning for unannotated data, whilst the latter focuses on fitting possible domain shift. (2) Both methods tend to learn the feature invariance before and after augmentation in the inferencing step, which serves as the foundation for updating segmentation network.

These similarities compel us to rethink and fuse consistency-based SSL and DG. Inspired by the class-level representation, we find that same organ shows class-level consistency between different domains. For an illustrative

example in Fig. 1 (bottom one row), the cardiac organ has strong similarity on both LGE and bSSFP domains. Accordingly, we propose domain diffusion augmentation. Specifically, we leverage distinct data augmentation strategies for global images and focal regions. The former is implemented to mitigate global domain shift, while the latter exploits the limited mask information to tailor and enhance class-level focal regions, replicating the class-specific shift. Moreover, we establish an augmentation scale-balancing mechanism to ensure the augmentation strategies remain informative and focused. The augmentation exponentially increase the data diversity compared to conventional, global-only data augmentation methods. Meanwhile, the augmented images are also set as different perturbations of consistency-based SSL, providing a unified framework of SSL and DG at the data level.

In the inference stage, we present a medical image segmentation model constructed from multiple branches. Specifically, we design a sharpening function to correct the probability outputs. The resulting statistical discrepancy of corrected probabilities is subsequently utilized to estimate pixel/voxel-level uncertainty via our proposed uncertainty evaluation method. This consistency loss with the uncertainty evaluation method fosters connections between different branches, facilitating decision-level fusion. Ultimately, to further reinforce the weight sharing across each branch, we employ an intermediate-level fusion method termed deep mutual learning strategy. The consistency constraint of different branches prompts model to capture domain invariant information and learn invariant features under different perturbations, providing a unified framework of SSL and DG at the model level.

The main contributions of this paper are summarized as follows: **(1)** We propose an SSL framework for medical segmentation that possesses cross-modality generalization ability, termed SSL-DG. It is a pioneer fusion of SSL and DG, addressing two core challenges: the scarcity of annotated data and the issue of domain shift. **(2)** We propose a domain diffusion augmentation for largely enriching domain diversity, which serves as a broad-spectrum, mask-based augmentation for medical image segmentation. **(3)** We propose an consistency loss based on uncertainty estimation. It evaluates the discrepancy between variant outputs generated from the same source data. Moreover, we propose a deep mutual learning strategy, which establishes a weight-sharing mechanism across multiple branches. The synthesis of these two strategies equips the model with the superior capability to learn from unannotated samples. **(4)** Extensive experiments on segmentation tasks show that SSL-DG has superior generalization and unannotated data learning capability.

Related Work

Consistency-based Semi-supervised Learning SSL harnesses the abundance of unannotated data to enhance model performance, significantly reducing the costs of manual annotation. Recently, consistency-based SSL has showcased impressive accuracy. For instance, MC-Net proposed a mutual consistency loss to train parallel networks [31], while URPC introduced uncertainty rectified pyramid consistency

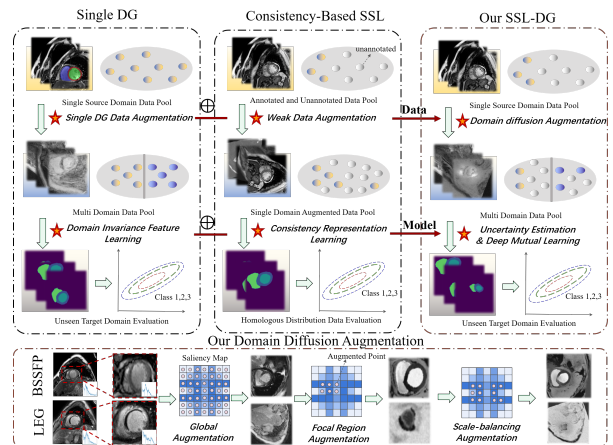


Figure 1: Conceptual overview of motivation of SSL-DG.

to train a segmentation network, using its multi-scale outputs to correct predictions for unannotated data [8]. Different from the previous works, we introduce additive class-level information into traditional data augmentation process of SSL and synergistically combines uncertainty estimation [39, 40, 41] with deep mutual strategy [34], prompting SSL model to learn domain invariant features.

Domain Generalization DG, relying on source domain data, forms models apt for direct generalization to target domains, addressing domain shift pragmatically [36, 50, 52]. Specific style transfer and data augmentation, which indirectly tackle potential changes on the target domain, are the most common methods [47, 51, 53]. However, these works often transfer and augment the global image, giving a restrained shift in data distribution [54, 55]. In this paper, we leverage distinct data augmentation strategies for global images and focal regions, exponentially increasing the data diversity.

Main Methodology

This section details the proposed SSL-DG. As depicted in Fig. 2, SSL-DG can be derived into three parts: domain diffusion augmentation, consistency loss based on uncertainty estimation, and deep mutual learning strategy.

Domain Diffusion Augmentation

Global and Focal Region Augmentation Imaging techniques such as computed tomography (CT) and magnetic resonance imaging (MRI) visualize lesions using distinct pixel mapping strategies, with salient features in alternating between light and dark. The tight coupling of deep learning models to the data sources hinders model’s cross-modality generalization [36]. Obtaining multi-modal medical images with pixel-level annotation is cost-prohibitive. Inspired by class-level representation and DG, we determine that unobserved target data can be approximated as a linear combination of source data at the class level, achieved by data augmentation. Therefore, we devise the domain diffusion augmentation to generate multi-modal images.

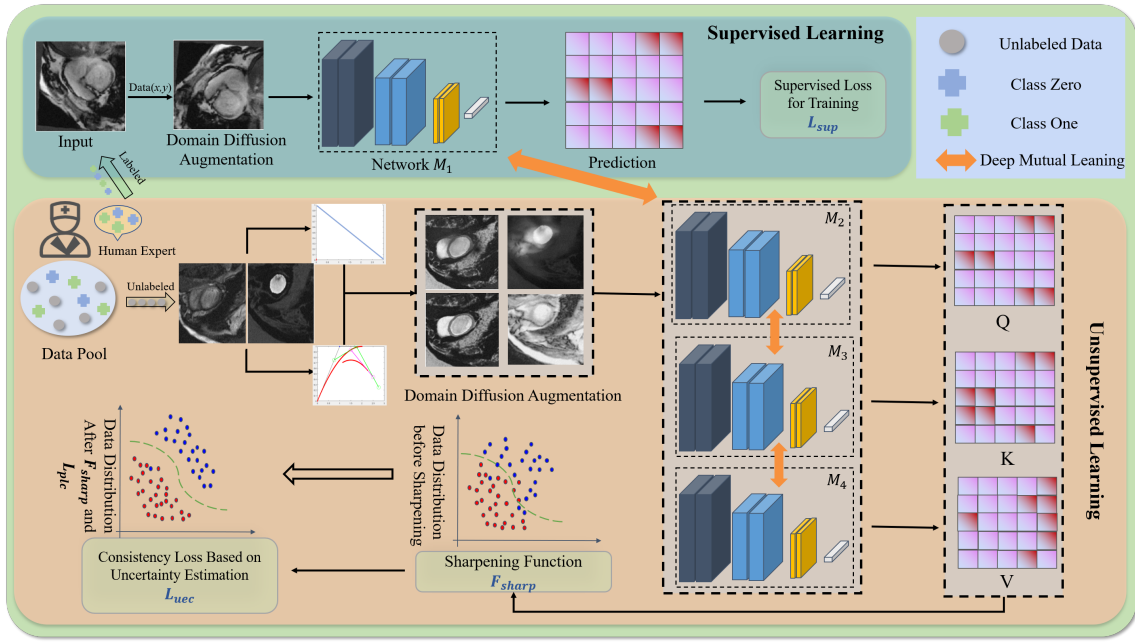


Figure 2: Workflow of the proposed SSL-DG.

The proposed augmentation is rooted in the deep semantic consistency across multimodal medical images of identical lesions. Beyond mere light and dark features, features extracted from images should be extended by incorporating pathological characteristics like shape, edge profile, and size. The pathological attributes convey more profound semantic information and maintain higher consistency across various imaging methods. Thus, by adjusting the distribution of pixel values, we promote the model to learn these deep semantic information, thereby improving the generalization performance.

Specifically, we define a monotonic non-linear transformation based on the Bézier curve, and the grayscale-inversion transformation, to adjust the pixel values of the original images. The mathematical expression of constrained Bézier curve can be given by:

$$B(k) = \sum_{i=0}^N \binom{N}{i} P_i (1-k)^{N-i} k^i, N=3, k \in [0, 1], \quad (1)$$

$$P = (a, b), a, b \in [0, 1], \quad (2)$$

where k denotes the ratio of the line's length and P represents the control point coordinates, set within the $[0, 1]$. In our study, two sets of curve control points are generated randomly from $[0, 1]$, with the starting and end points of both sets fixed at $(0, 0)$, $(1, 1)$. Contrastingly, the grayscale-inversion transformation produces images that are stark opposites, leading to difficulties in feature extraction. Its representation is:

$$g(x, y) = T - f(x, y), \quad (3)$$

where T is the maximum pixel value of image, f is the pixel value of the current position, x, y are the coordinate positions. Using pixel-level transformation, we define the Global

Augmentation (GA) and Focal region Augmentation (FA). Prior to augmentations, the pixel values of input data are normalized to $[0, 1]$. The monotonic non-linear and grayscale-inversion transformation is tagged as $\Lambda(\cdot)$ and $\Gamma(\cdot)$, respectively. The GA is described as:

$$O^{GA} = \eta(P_1 \Lambda_+(x) \odot P_{0.1} \Gamma(x)) + \mu, \quad (4)$$

$$P_\gamma = \begin{cases} 1, & \text{if } \text{random}(0, 1) \leq \gamma \\ 0, & \text{else} \end{cases} \quad (5)$$

where $\eta \sim \mathcal{TN}(1, \sigma_1)$, $\mu \sim \mathcal{TN}(0, \sigma_2)$ are GA factors, and σ_1 and σ_2 are standard deviations of the two truncated Gaussian distributions, respectively. Λ_+ implies the Bézier curve function performing forward mapping exclusively. \odot indicates mutually exclusive events (which is inactive in the case of monotonic non-linear transformation). The FA, utilizing the masks of training data, accomplishes class-level augmentation, which is described as:

$$O^{FA} = \sum_{n=0}^N \eta_n \psi_n \Lambda(x) + \mu_n. \quad (6)$$

where $\eta_n \sim \mathcal{TN}(1, \sigma_1)$ and $\mu_n \sim \mathcal{TN}(0, \sigma_2)$ are FA factors. N denotes all class number including background ($n=0$). We set $\psi_0 = 1$ to ensure the O^{FA} is dissimilar with O^{GA} , and for $n \neq 0$, we set $\psi_n = 0.5$. For the FA, the background represents the non-blank regions (the human body areas). And each class is augmented with independent parameters. The focal region and background classification depend on the mask of the original image. This mask-based augmentation scales the domain distribution, often exponentially, with the generated data.

Augmentation Scale-balancing Mechanism There is an uncertainty arising from the random FA and is a consequence of constraints lacking. This can escalate computational costs during model training and may significantly impair performance. To address this, we propose an augmentation scale-balancing mechanism to integrate global and focal region augmented medical images. This can be achieved using a combination of gradient calculation and saliency feature mapping:

$$(\bar{O}^{GA}, \bar{O}^{FA}, \bar{m}) = \mathcal{H}(O^{GA}, O^{FA}, m), \quad (7)$$

$$G = \nabla_{\bar{O}^{GA}} \mathcal{L}(M_{\Phi}(\bar{O}^{GA}), \bar{m}), \quad (8)$$

$$S = L_2(\mathcal{F}(G)), \quad (9)$$

$$\bar{O}^{SBA} = S \times \bar{O}^{GA} + (1 - S) \times \bar{O}^{FA}. \quad (10)$$

where \mathcal{H} denotes the weak augmentation [30], m refers to the mask of data, \mathcal{L} is the training loss, M_{Φ} is the segmentation model, L_2 denotes the l_2 normalization. \mathcal{F} represents a smooth process, which applies l_2 normalization to gradient values and reduces the gradient values map to a grid size of $g \times g$. Following this, the process uses quadratic B-spline kernels to interpolate to the original image size. We present a visual overview of domain diffusion augmentation in Fig. 1.

The augmentation scale-balancing mechanism amalgamates global and focal region augmented images, and is linearly related to these augmented data. In this case, FA can be controlled by gradient calculation. The linear behavior mitigates undesirable oscillations during out-of-distribution prediction, compared to directly inputting focal region augmented samples. Thus, we take \bar{O}^{GA} and \bar{O}^{SBA} as input.

Consistency Loss Based on Uncertainty Estimation

As shown in Fig. 3, the segmentation model of SSL-DG consists of multiple branches, each with an independent decoder. For improved efficiency, shared encoders are adopted. The model accepts pre- and post-augmented samples, subsequently outputting the probability of containing lesions at each pixel. And outputs of augmented images from the same source are similar if the input sources are identical. This prior knowledge prompts us to propose the consistency loss based on uncertainty estimation.

Sharpening Function First, we devise a sharpening function F_{sharp} , inspired by the entropy minimization loss [37, 38], to adjust the output probability distribution. The loss optimizes the decision boundary by distancing samples from the decision surface, yielding more confident segmentation results. We introduce this concept to modify the output layer so as to rectify the outputs' probability distribution. Without extra training or computation, the sharpening function enhances classification confidence for samples near the decision surface, thus maintaining the efficacy of the consistency loss based on uncertainty estimation.

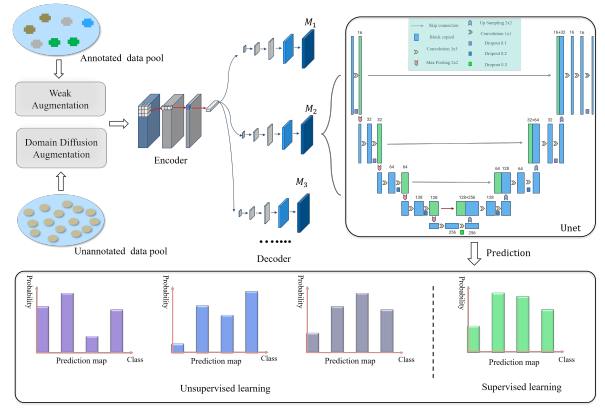


Figure 3: Diagram of segmentation model architecture.

$$p'(y|x; \varepsilon_m) = \frac{p(y|x; \varepsilon_m)^{1/T}}{p(y|x; \varepsilon_m)^{1/T} + (1 - p(y|x; \varepsilon_m))^{1/T}}. \quad (11)$$

where x is the input of segmentation model. ε_m is the parameter of the network M_m , and $p(y|x; \varepsilon_m)$ is the output of the network M_m . T represents the hyper-parameter to control the temperature of sharpening.

Uncertainty evaluation method Based on $p'(y|x; \varepsilon_m)$, a novel method is formulated to assess uncertainty within the SSL-DG, which is delineated as:

$$p_{avg}^i = \sum_{m=2}^k p_m^i, \quad (12)$$

$$U_m^i = \sum_{m=1}^k p_m^i \cdot \log \frac{p_m^i}{p_{avg}^i}, \quad (13)$$

where k symbolizes the total number of segmentation branches. p_m^i signifies the probability of pixel i belong to the organs. U_m^i is the uncertainty of pixel i at the output of M_m . And p_{avg}^i represents the outputs' average probabilities.

Uncertainty at the output of M_m is calculated by determining the difference between p_m^i and p_{avg}^i . We performed uncertainty estimations on multiple branches within the self-supervised learning domain to yield the uncertainty estimation set U_M .

$$U_m = \frac{1}{N} \sum_{i=1}^N p_m^i. \quad (14)$$

where N corresponds to the total pixels in the image.

Consistency Loss Based on the proposed uncertainty evaluation method, we further construct the uncertainty estimation loss L_{unc} and the uncertainty revised loss L_{urm} . And the sum of L_{uec} and L_{unr} provides the consistency loss based on uncertainty estimation L_{uec} , defined as:

$$L_{uec} = \partial L_{unc} + (1 - \partial)L_{unr}, \quad (15)$$

$$L_{une} = \frac{1}{k-1} \sum_{m=2}^k U_m, \quad (16)$$

$$L_{unr} = \frac{1}{k-1} \sum_{m=2}^k \frac{\sum_{i=1}^N \|p_m^i - p_{avg}^i\|_2 \cdot \varpi_m^i}{\sum_{i=1}^N \varpi_m^i}. \quad (17)$$

where ∂ is the weights to balance the impact of the L_{une} and L_{unr} . k is the total number of branches. ϖ_m^i is a rectifying weight, which can be defined as $\varpi_m^i = e^{-U_m^i}$. The aim of L_{unr} is to emphasize reliable parts and ignore unreliable parts of the predictions for stable self-supervised training. L_{une} works to decrease prediction entropy, furtherly boosting the method’s robustness and generalization.

Deep Mutual Learning Strategy

The consistency loss based on uncertainty estimation establishes the connection between various branches’ outputs, corresponding to decision-level fusion. To augment weight sharing within each branch, we devise an intermediate weight-sharing strategy termed deep mutual learning L_{wsm} , as the intermediate-level fusion. It takes $p(y_{output}|x, \varepsilon_m)$ as input and establishes a weight-sharing mechanism for different segmentation networks via Mean Squared Error loss.

$$L_{wsm} = \frac{1}{N(k-2)} \sum_{m=2, m \neq j}^k \sum_{i=1}^N (p(y_j|x, \varepsilon_j) - p(y_i|x, \varepsilon_m))^2, \quad (18)$$

where k is the total number of branches in the segmentation model, $p(y_i|x, \varepsilon_m)$ is the probability obtained by branch M_m of pixel i belong to the lesion or organ.

The Overall Objective Loss Function

We merge consistency loss based on uncertainty estimation and mutual learning strategies as the overall loss of self-supervised learning. SSL-DG incorporates both fully supervised and self-supervised learning. Consequently, we use a weighted amalgamation of these two components, encapsulated in Eq. 20. Note that the L_{sup} is the Dice loss, and μ is tradeoff weights responsible for balancing the influence of two terms.

$$L_{unsup} = \gamma L_{uec} + (1 - \gamma) L_{wsm}, \quad (19)$$

$$L_{total} = \mu L_{sup} + (1 - \mu) L_{unsup}. \quad (20)$$

Experiment and Results

Data and Processing

We assess the performance of SSL-DG using cross-modality abdominal datasets[43, 44] and cross-sequence cardiac datasets [45]. Our dataset division and pre-processing method are based on the procedures outlined by [46]. To provide a more in-depth understanding of our experiments, we will open-source relevant code. During data processing, we adopt the weak augmentation [30], which encompass

Affine, Elastic, Brightness, Contrast, Gamma, and Additive Gaussian Noise. And domain diffusion augmentation is used as additional stages after the weak augmentation. To maintain a fair comparative ground, all competing methods use the weak augmentation. Additionally, it is noteworthy that scholarly investigations to date have predominantly concentrated on individual aspects of SSL or DG. However, a holistic approach that synergistically amalgamates these dual aspects remains largely unexplored. Thus, in assessing the performance of SSL-DG, we proceed by independently contrasting it with both SSL and DG.

Implementation Details

We develop a segmentation network underpinned by the U-Net architecture, which is trained initio, eschewing the use of pre-training. The grid sizes g for abdominal and cardiac datasets are empirically determined at 3 and 18, respectively. Each dataset is processed in batch size of 16, composed of an equal split between annotated and unannotated patches. Optimization is performed using the Adam with a set initial learning rate of 5×10^{-3} and a weight decay factor of 3×10^{-5} . The framework is deployed on a workstation furnished with a NVIDIA GeForce RTX 3080 GPU, possessing a memory capacity of 10G.

Results and Comparative Analysis

Quantitative Comparision To substantiate the superiority of our proposed SSL-DG, we benchmark its performance against an array of state-of-the-art DG and SSL methodologies, including Feddg [47], Sdn [36], SLAug [46], SASS-NeT [48], DTC [49], and MC-net+ [31]. These methods are applied across a variety of annotated data configurations to demonstrate the heightened robustness and generalization of SSL-DG. To ensure fair comparison, the weak augmentation is utilized across all methods. The performances of U-net with varying annotated samples on the target domain are also reported, acting as an upper bound. The Dice score is deployed as the principal evaluation metric for gauging instance segmentation.

The quantitative performance of SSL-DG and the compared methods is presented in Tab. 1 and 2. With the application of 50% annotated samples, SSL-DG enhances the Dice score by 5.77% relative to the most recent standalone DG work, SLAug, on the target domain MRI. Additionally, as the proportion of annotated samples is diminished further, the preeminence of SSL-DG becomes increasingly apparent. This phenomenon also can be observed on other target domains. Notably, on the target domain LGE, SSL-DG surpasses the upper bound of performance with the application of 50% annotated samples. This highlights SSL-DG’s capability to address domain shift and its effectiveness in unannotated data feature learning. The performance of SSL methodologies devoid of domain adaptation is markedly lower. The domain shift across disparate multimodals precipitated a severe degradation in the performance of the SSL model. Overall, the experimental findings affirm that SSL-DG delivers superior results across evaluation metrics, and significantly outpaces its competitors in Dice score when equal numbers of annotated samples are used. Moreover, we

Method	Venue	#Scans Used		Abdominal CT-MRI					Cardiac bSSFP-LGE			
		X_l	X_u	Liver	R-Kidney	L-Kidney	Spleen	Average	LVC	MYO	RVC	Average
U-net (target)	-	10%	0	69.90	72.65	70.42	70.76	70.93	58.03	50.83	62.77	57.21
U-net (target)	-	20%	0	83.51	83.73	79.86	82.39	82.37	75.45	74.02	71.45	73.64
U-net (target)	-	50%	0	86.19	88.09	83.12	86.95	86.10	84.83	78.55	78.64	80.67
U-net (target)	-	100%	0	91.30	92.43	89.86	89.83	90.85	92.04	83.11	89.30	88.15
Feddg	CVPR' 2021	20%	0	61.56	70.32	63.86	63.05	64.70	68.71	62.24	69.93	66.96
Sadn	CVPR' 2022	-	-	64.51	64.85	69.92	62.33	65.40	72.63	64.44	71.79	69.62
SLAug	AAAI' 2023	-	-	66.34	64.09	61.40	70.96	65.95	71.58	68.03	77.75	72.45
D	Feddg	-	50%	73.98	78.71	78.98	75.03	76.68	81.73	77.42	77.94	79.03
G	Sadn	-	-	83.45	82.91	80.41	73.01	79.95	85.37	74.62	82.78	80.92
	SLAug	-	-	81.32	83.78	78.12	77.65	80.22	92.01	81.25	83.07	85.44
	Feddg	-	100%	77.66	77.35	81.81	80.37	79.30	84.71	78.95	82.46	82.04
	Sadn	-	-	88.74	88.77	85.92	81.35	86.20	92.30	81.07	86.00	86.46
	SLAug	-	-	90.08	89.23	87.54	87.67	88.63	91.53	80.65	87.90	86.69
SASSNeT	MICCAI' 2020	10%	90%	28.07	29.87	21.91	30.46	27.58	8.79	29.60	21.55	19.98
DTC	AAAI' 2021	-	-	30.4	17.33	35.02	16.84	24.90	38.12	38.22	45.91	40.75
MC-Net+	MedIA' 2022	-	-	33.02	20.82	35.35	26.01	28.80	33.92	32.03	29.02	31.66
S	SASSNeT	-	20%	30.65	31.67	35.74	35.32	33.35	33.05	39.98	48.08	40.57
S	DTC	-	-	33.79	22.50	38.1	28.09	30.62	44.83	50.24	53.33	49.47
L	MC-Net+	-	-	42.53	35.7	31.98	36.85	36.77	43.97	48.3	49.12	47.13
	SASSNeT	-	50%	40.42	40.48	39.87	37.06	39.46	35.32	41.28	49.78	42.19
	DTC	-	-	41.88	45.95	42.56	34.46	41.21	46.27	53.33	56.80	52.13
	MC-Net+	-	-	54.67	50.24	40.06	41.55	46.63	51.02	53.49	50.82	51.78
O	SSL-DG	10%	90%	79.36	82.16	79.18	80.70	80.35	86.24	73.25	76.76	78.75
U	SSL-DG	20%	80%	<u>85.56</u>	<u>85.50</u>	<u>81.98</u>	<u>82.82</u>	<u>83.97</u>	<u>90.41</u>	<u>78.84</u>	<u>84.41</u>	<u>84.56</u>
R	SSL-DG	50%	50%	87.59	85.75	85.69	84.93	85.99	91.18	80.11	86.33	85.87

Table 1: Performance comparison of different method on the target domain MRI and LGE. Dice score (%) is used as the evaluation metrics. X_l denote the annotated samples and X_u denote the unannotated samples. The top performance for 20% annotated samples is highlighted in bold, and for 50% annotated samples, it's underlined.

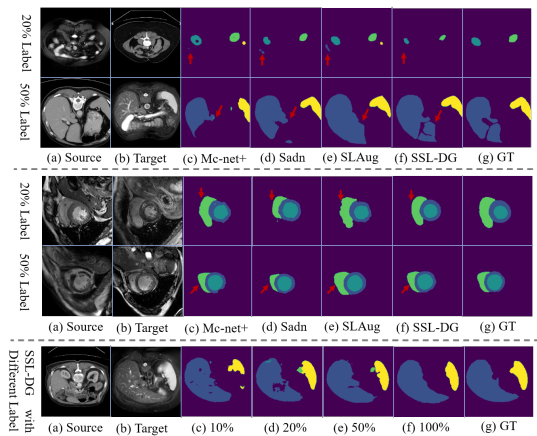


Figure 4: Qualitative comparison on the target domain MRI (top two rows) and LGE (middle two rows). And qualitative comparison under different annotated samples settings (bottom one row).

also performed statistical tests on the results. The t-test results (with p-value < 0.05) indicate that our method's performance benefits are statistically significant in all cases.

Visual Comparison In Fig. 4, we present the qualitative outcomes of various methods, including MC-net+, Sadn, SLAug, and SSL-DG. Concurrently, we report the segmentation results of SSL-DG under varied annotated sample settings. The results suggest that SSL-DG adeptly segments salient organs, accommodating a broad range of sizes,

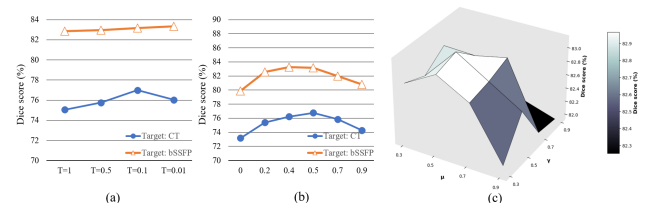


Figure 5: (a) Performance of SSL-DG w.r.t. T . (b) Performance of SSL-DG w.r.t. α . (c) Performance of SSL-DG w.r.t. μ and γ .

shapes, and locations. Notably, the object boundaries delineated by our method exhibit enhanced clarity compared to other benchmark methods.

Ablation Study

Effectiveness of Domain Diffusion Augmentation We assess domain diffusion augmentation's impact on SSL-DG using 20% annotated samples. As shown in Tab. 3, GA and FA enhance baseline by significant margins (Dice scores: +9.52 and +9.46) on the target domain CT. This highlights the proposed augmentation's effectiveness to improve model generalization. Comparing results of #3 and #5, replacing FA with SBA boosts performance by 3.6%. This indicates the scale-balancing strategy effectively directs data augmentation, setting a rigorous generalization boundary. In sum, the GA, FA, and SBA promote mutually and are all indispensable for the superior domain generalization.

Method	Venue	#Scans Used		Abdominal MRI-CT					Cardiac LGE-bSSFP			
		X_l	X_u	Liver	R-Kidney	L-Kidney	Spleen	Avg	LVC	MYO	RVC	Avg
U-net (target)	-	10%	0	69.50	73.72	76.61	70.94	72.69	70.85	58.70	60.05	63.20
U-net (target)	-	20%	0	80.32	84.05	86.24	80.32	82.73	79.62	72.66	79.42	77.25
U-net (target)	-	50%	0	85.14	88.94	88.01	85.36	86.86	85.27	80.75	85.90	83.97
U-net (target)	-	100%	0	98.87	92.11	91.75	88.55	89.74	91.16	82.93	90.39	88.16
Feddg	CVPR' 2021	20%	0	51.86	49.67	52.92	61.72	54.04	50.74	40.91	52.86	48.17
Sadn	CVPR' 2022	-	-	67.51	62.80	71.84	75.01	69.29	62.33	54.32	67.30	61.32
SLAug	AAAI' 2023	-	-	68.75	62.13	74.64	77.63	70.79	58.77	59.53	67.33	61.88
D Feddg	-	50%	0	70.39	71.02	72.74	77.89	73.01	61.52	63.69	70.33	65.18
G Sadn	-	-	-	77.46	86.56	84.00	80.78	82.20	71.36	60.24	70.06	67.22
SLAug	-	-	-	82.87	84.92	81.33	80.90	82.51	74.86	70.02	78.54	74.47
Feddg	-	100%	0	83.65	82.92	79.89	82.07	82.13	75.69	73.02	75.48	74.73
Sadn	-	-	-	89.79	88.02	83.10	86.41	86.83	85.39	81.61	86.80	84.60
SLAug	-	-	-	90.08	86.23	84.54	85.67	86.63	91.53	80.65	87.90	86.69
SASSNeT	MICCAI' 2020	10%	90%	15.89	16.69	27.35	22.01	20.49	11.26	28.79	27.35	22.53
DTC	AAAI' 2021	-	-	19.86	15.01	29.83	19.77	21.12	20.58	35.98	37.53	31.36
MC-Net+	MedIA' 2022	-	-	20.47	20.62	27.05	18.89	21.76	34.84	35.54	29.72	35.97
S SASSNeT	-	20%	80%	25.74	23.88	33.04	28.92	27.90	28.75	39.02	42.11	36.63
S DTC	-	-	-	30.02	39.91	30.70	30.76	32.85	38.00	42.08	49.68	43.25
L MC-Net+	-	-	-	40.32	38.01	43.99	38.65	40.24	42.57	42.38	48.70	44.55
SASSNeT	-	50%	50%	28.45	30.95	37.47	37.04	33.48	31.91	40.67	44.78	39.12
DTC	-	-	-	35.94	50.94	33.66	32.09	38.16	41.42	43.61	51.23	45.42
MC-Net+	-	-	-	54.67	53.24	45.08	42.30	48.82	43.56	52.96	50.94	49.15
O SSL-DG	-	10%	90%	74.59	62.98	65.54	64.45	66.89	80.53	73.79	78.02	77.45
U SSL-DG	-	20%	80%	<u>80.52</u>	<u>78.89</u>	<u>77.26</u>	71.25	<u>76.98</u>	<u>88.75</u>	<u>77.11</u>	<u>83.59</u>	<u>83.15</u>
R SSL-DG	-	50%	50%	88.28	80.41	85.92	85.27	84.97	90.92	80.02	85.05	85.33

Table 2: Performance comparison of different method on the target domain CT and bSSFP. Dice score (%) is used as the evaluation metrics. X_l denote the annotated samples and X_u denote the unannotated samples. The top performance for 20% annotated samples is highlighted in bold, and for 50% annotated samples, it's underlined.

Methods	GA	FA	SBA	MRI-CT	LGE-bSSFP
Baseline	✗	✗	✗	42.52	49.31
#1	✓	✗	✗	52.03	67.29
#2	✗	✓	✗	51.98	70.43
#3	✓	✓	✗	73.05	79.80
#4	✗	✓	✓	64.99	81.77
#5	✓	✗	✓	76.65	82.68
SSL-DG	✓	✓	✓	76.98	83.15

Methods	F_{sharp}	L_{une}	L_{wsm}	MRI-CT	LGE-bSSFP
Baseline	✗	✗	✗	71.25	78.90
#6	✓	✗	✗	72.35	79.11
#7	✗	✓	✗	74.32	83.02
#8	✗	✗	✓	72.23	79.65
#9	✓	✓	✗	75.32	82.73
#10	✗	✓	✓	76.04	82.56
#11	✓	✗	✓	73.2	79.85
SSL-DG	✓	✓	✓	76.98	83.15

Table 3: Ablation study of Domain Diffusion Augmentation, Consistency Loss based on Uncertainty Estimation and Deep Mutual Learning Strategy

Effectiveness of Consistency Loss based on Uncertainty Estimation and Deep Mutual Learning Strategy To access the efficacy of the proposed consistency loss and deep mutual learning strategy, we benchmarked it against various alternative configurations. As shown in Tab. 3, compared with Baseline, the integration of L_{une} yields a notable enhancement in the Dice score: an increment of 3.07% on the target domain CT and 4.12% on bSSFP. Solely incorporating the F_{sharp} or L_{wsm} offers marginal advancement in performance. The results underscore the pivotal role of uncertainty evaluation in bolstering SSL capabilities. SSL-DG, which synergistically leverages all three modules, outperforms its counterparts.

Adjustment T , α , μ and γ T is the hyper-parameter to control the temperature of sharpening. α , μ and γ are utilized to balance the overall loss. As shown in Fig. 5, the experimental results show that SSL-DG achieves the best performance with T at 0.1 and α , μ and γ each at 0.5.

Conclusions

In this paper, we address two core challenges in current medical image segmentation: the scarcity of annotated data and the issue of domain shift. We present SSL-DG, a novel segmentation framework that integrates domain diffusion augmentation, consistency loss based on uncertainty estimation, and a deep mutual learning strategy. To the best of our knowledge, SSL-DG represents the inaugural SSL framework for medical image segmentation with cross-modality generalization ability. Experimental results verify that SSL-DG outperforms leading methods.

References

- [1] A. Hering, L. Hansen, T. C. Mok, A. C. Chung, H. Siebert, S. Häger, A. Lange, S. Kuckertz, S. Heldmann, W. Shao *et al.*, “Learn2reg: comprehensive multi-task medical image registration challenge, dataset and evaluation in the era of deep learning,” *IEEE Transactions on Medical Imaging*, vol. 42, no. 3, pp. 697–712, 2022.
- [2] O. Dalmaz, M. Yurt, and T. Çukur, “Resvit: Residual vision transformers for multimodal medical image synthesis,” *IEEE Transactions on Medical Imaging*, vol. 41, no. 10, pp. 2598–2614, 2022.
- [3] Y. Tang, D. Yang, W. Li, H. R. Roth, B. Landman, D. Xu, V. Nath, and A. Hatamizadeh, “Self-supervised pre-training of swin transformers for 3d medical image analysis,” in *Proceedings of the IEEE/CVF Conference on Computer Vision and Pattern Recognition*, 2022, pp. 20730–20740.
- [4] C. You, Y. Zhou, R. Zhao, L. Staib, and J. S. Duncan, “Simcvd: Simple contrastive voxel-wise representation distillation for semi-supervised medical image segmentation,” *IEEE Transactions on Medical Imaging*, vol. 41, no. 9, pp. 2228–2237, 2022.
- [5] R. Selvan, N. Bhagwat, L. F. Wolff Anthony, B. Kanding, and E. B. Dam, “Carbon footprint of selecting and training deep learning models for medical image analysis,” in *International Conference on Medical Image Computing and Computer-Assisted Intervention*. Springer, 2022, pp. 506–516.
- [6] H. A. Haenssle, C. Fink, R. Schneiderbauer, F. Toberer, T. Buhl, A. Blum, A. Kalloo, A. B. H. Hassen, L. Thomas, A. Enk *et al.*, “Man against machine: diagnostic performance of a deep learning convolutional neural network for dermoscopic melanoma recognition in comparison to 58 dermatologists,” *Annals of oncology*, vol. 29, no. 8, pp. 1836–1842, 2018.
- [7] X. Liu, L. Faes, A. U. Kale, S. K. Wagner, D. J. Fu, A. Bruynseels, T. Mahendiran, G. Moraes, M. Shandas, C. Kern *et al.*, “A comparison of deep learning performance against health-care professionals in detecting diseases from medical imaging: a systematic review and meta-analysis,” *The lancet digital health*, vol. 1, no. 6, pp. e271–e297, 2019.
- [8] X. Luo, G. Wang, W. Liao, J. Chen, T. Song, Y. Chen, S. Zhang, D. N. Metaxas, and S. Zhang, “Semi-supervised medical image segmentation via uncertainty rectified pyramid consistency,” *Medical Image Analysis*, vol. 80, p. 102517, 2022.
- [9] Y. Wang, J. Peng, and Z. Zhang, “Uncertainty-aware pseudo label refinery for domain adaptive semantic segmentation,” in *Proceedings of the IEEE/CVF International Conference on Computer Vision*, 2021, pp. 9092–9101.
- [10] D.-H. Lee *et al.*, “Pseudo-label: The simple and efficient semi-supervised learning method for deep neural networks,” in *Workshop on challenges in representation learning*, 2013, p. 896.
- [11] A. Tarvainen and H. Valpola, “Mean teachers are better role models: Weight-averaged consistency targets improve semi-supervised deep learning results,” *Advances in neural information processing systems*, vol. 30, 2017.
- [12] J. Jeong, S. Lee, J. Kim, and N. Kwak, “Consistency-based semi-supervised learning for object detection,” *Advances in neural information processing systems*, vol. 32, 2019.
- [13] J. Sourati, A. Gholipour, J. G. Dy, X. Tomas-Fernandez, S. Kurugol, and S. K. Warfield, “Intelligent labeling based on fisher information for medical image segmentation using deep learning,” *IEEE transactions on medical imaging*, vol. 38, no. 11, pp. 2642–2653, 2019.
- [14] P. Jiang, S. Huang, Z. Fu, Z. Sun, T. M. Lakowski, and P. Hu, “Deep graph embedding for prioritizing synergistic anticancer drug combinations,” *Computational and structural biotechnology journal*, vol. 18, pp. 427–438, 2020.
- [15] O. Ronneberger, P. Fischer, and T. Brox, “U-net: Convolutional networks for biomedical image segmentation,” in *Medical Image Computing and Computer-Assisted Intervention—MICCAI 2015: 18th International Conference, Munich, Germany, October 5-9, 2015, Proceedings, Part III 18*. Springer, 2015, pp. 234–241.
- [16] Z. Zhou, M. M. Rahman Siddiquee, N. Tajbakhsh, and J. Liang, “Unet++: A nested u-net architecture for medical image segmentation,” in *Deep Learning in Medical Image Analysis and Multimodal Learning for Clinical Decision Support: 4th International Workshop, DLMIA 2018, and 8th International Workshop, ML-CDS 2018, Held in Conjunction with MICCAI 2018, Granada, Spain, September 20, 2018, Proceedings 4*. Springer, 2018, pp. 3–11.
- [17] Ö. Çiçek, A. Abdulkadir, S. S. Lienkamp, T. Brox, and O. Ronneberger, “3d u-net: learning dense volumetric segmentation from sparse annotation,” in *Medical Image Computing and Computer-Assisted Intervention—MICCAI 2016: 19th International Conference, Athens, Greece, October 17-21, 2016, Proceedings, Part II 19*. Springer, 2016, pp. 424–432.
- [18] H. Cao, Y. Wang, J. Chen, D. Jiang, X. Zhang, Q. Tian, and M. Wang, “Swin-unet: Unet-like pure transformer for medical image segmentation,” in *European conference on computer vision*. Springer, 2022, pp. 205–218.
- [19] I. Qureshi, J. Yan, Q. Abbas, K. Shaheed, A. B. Riaz, A. Wahid, M. W. J. Khan, and P. Szczuko, “Medical image segmentation using deep semantic-based methods: A review of techniques, applications and emerging trends,” *Information Fusion*, 2022.
- [20] M. Aljabri and M. AlGhamdi, “A review on the use of deep learning for medical images segmentation,” *Neurocomputing*, 2022.

- [21] C. Shorten and T. M. Khoshgoftaar, "A survey on image data augmentation for deep learning," *Journal of big data*, vol. 6, no. 1, pp. 1–48, 2019.
- [22] A. H. Barshooi and A. Amirkhani, "A novel data augmentation based on gabor filter and convolutional deep learning for improving the classification of covid-19 chest x-ray images," *Biomedical Signal Processing and Control*, vol. 72, p. 103326, 2022.
- [23] K. Chaitanya, N. Karani, C. F. Baumgartner, E. Erdil, A. Becker, O. Donati, and E. Konukoglu, "Semi-supervised task-driven data augmentation for medical image segmentation," *Medical Image Analysis*, vol. 68, p. 101934, 2021.
- [24] K. He, X. Zhang, S. Ren, and J. Sun, "Deep residual learning for image recognition," in *Proceedings of the IEEE conference on computer vision and pattern recognition*, 2016, pp. 770–778.
- [25] A. Vaswani, N. Shazeer, N. Parmar, J. Uszkoreit, L. Jones, A. N. Gomez, Ł. Kaiser, and I. Polosukhin, "Attention is all you need," *Advances in neural information processing systems*, vol. 30, 2017.
- [26] D. Jha, P. H. Smedsrud, M. A. Riegler, D. Johansen, T. De Lange, P. Halvorsen, and H. D. Johansen, "Resunet++: An advanced architecture for medical image segmentation," in *2019 IEEE international symposium on multimedia (ISM)*. IEEE, 2019, pp. 225–2255.
- [27] F. Milletari, N. Navab, and S.-A. Ahmadi, "V-net: Fully convolutional neural networks for volumetric medical image segmentation," in *2016 fourth international conference on 3D vision (3DV)*. Ieee, 2016, pp. 565–571.
- [28] J. Chen, Y. Lu, Q. Yu, X. Luo, E. Adeli, Y. Wang, L. Lu, A. L. Yuille, and Y. Zhou, "Transunet: Transformers make strong encoders for medical image segmentation," *arXiv preprint arXiv:2102.04306*, 2021.
- [29] F. Bougourzi, C. Distanto, F. Dornaika, and A. Taleb-Ahmed, "Pdatt-unet: Pyramid dual-decoder attention unet for covid-19 infection segmentation from ct-scans," *Medical Image Analysis*, vol. 86, p. 102797, 2023.
- [30] K. Sohn, D. Berthelot, N. Carlini, Z. Zhang, H. Zhang, C. A. Raffel, E. D. Cubuk, A. Kurakin, and C.-L. Li, "Fixmatch: Simplifying semi-supervised learning with consistency and confidence," *Advances in neural information processing systems*, vol. 33, pp. 596–608, 2020.
- [31] Y. Wu, Z. Ge, D. Zhang, M. Xu, L. Zhang, Y. Xia, and J. Cai, "Mutual consistency learning for semi-supervised medical image segmentation," *Medical Image Analysis*, vol. 81, p. 102530, 2022.
- [32] D. Berthelot, N. Carlini, I. Goodfellow, N. Papernot, A. Oliver, and C. A. Raffel, "Mixmatch: A holistic approach to semi-supervised learning," *Advances in neural information processing systems*, vol. 32, 2019.
- [33] Y. Zhang, T. Xiang, T. M. Hospedales, and H. Lu, "Deep mutual learning," in *Proceedings of the IEEE conference on computer vision and pattern recognition*, 2018, pp. 4320–4328.
- [34] H. Zhao, G. Yang, D. Wang, and H. Lu, "Deep mutual learning for visual object tracking," *Pattern Recognition*, vol. 112, p. 107796, 2021.
- [35] R. Wu, M. Feng, W. Guan, D. Wang, H. Lu, and E. Ding, "A mutual learning method for salient object detection with intertwined multi-supervision," in *Proceedings of the IEEE/CVF conference on computer vision and pattern recognition*, 2019, pp. 8150–8159.
- [36] Z. Zhou, L. Qi, X. Yang, D. Ni, and Y. Shi, "Generalizable cross-modality medical image segmentation via style augmentation and dual normalization," in *Proceedings of the IEEE/CVF Conference on Computer Vision and Pattern Recognition*, 2022, pp. 20856–20865.
- [37] T.-H. Vu, H. Jain, M. Bucher, M. Cord, and P. Pérez, "Advent: Adversarial entropy minimization for domain adaptation in semantic segmentation," in *Proceedings of the IEEE/CVF conference on computer vision and pattern recognition*, 2019, pp. 2517–2526.
- [38] Y. Grandvalet and Y. Bengio, "Semi-supervised learning by entropy minimization," *Advances in neural information processing systems*, vol. 17, 2004.
- [39] M. S. Ayhan, L. Kühlewein, G. Aliyeva, W. Inhoffen, F. Ziemssen, and P. Berens, "Expert-validated estimation of diagnostic uncertainty for deep neural networks in diabetic retinopathy detection," *Medical image analysis*, vol. 64, p. 101724, 2020.
- [40] J. Gawlikowski, C. R. N. Tassi, M. Ali, J. Lee, M. Humt, J. Feng, A. Kruspe, R. Triebel, P. Jung, R. Roscher *et al.*, "A survey of uncertainty in deep neural networks," *Artificial Intelligence Review*, pp. 1–77, 2023.
- [41] Z. Zheng and Y. Yang, "Rectifying pseudo label learning via uncertainty estimation for domain adaptive semantic segmentation," *International Journal of Computer Vision*, vol. 129, no. 4, pp. 1106–1120, 2021.
- [42] C. H. Sudre, W. Li, T. Vercauteren, S. Ourselin, and M. Jorge Cardoso, "Generalised dice overlap as a deep learning loss function for highly unbalanced segmentations," in *Deep Learning in Medical Image Analysis and Multimodal Learning for Clinical Decision Support: Third International Workshop, DLMIA 2017, and 7th International Workshop, ML-CDS 2017, Held in Conjunction with MICCAI 2017, Québec City, QC, Canada, September 14, Proceedings 3*. Springer, 2017, pp. 240–248.
- [43] A. E. Kavur, N. S. Gezer, M. Barış, S. Aslan, P.-H. Conze, V. Groza, D. D. Pham, S. Chatterjee, P. Ernst, S. Özkan *et al.*, "Chaos challenge-combined (ct-mr) healthy abdominal organ segmentation," *Medical Image Analysis*, vol. 69, p. 101950, 2021.
- [44] B. Landman, Z. Xu, J. Igelsias, M. Styner, T. Langerak, and A. Klein, "Miccai multi-atlas labeling beyond the cranial vault—workshop and challenge," in *Proc. MICCAI Multi-Atlas Labeling Beyond Cranial Vault—Workshop Challenge*, vol. 5, 2015, p. 12.

- [45] X. Zhuang, J. Xu, X. Luo, C. Chen, C. Ouyang, D. Rueckert, V. M. Campello, K. Lekadir, S. Vesal, N. RaviKumar *et al.*, “Cardiac segmentation on late gadolinium enhancement mri: a benchmark study from multi-sequence cardiac mr segmentation challenge,” *Medical Image Analysis*, vol. 81, p. 102528, 2022.
- [46] Z. Su, K. Yao, X. Yang, K. Huang, Q. Wang, and J. Sun, “Rethinking data augmentation for single-source domain generalization in medical image segmentation,” in *Proceedings of the AAAI Conference on Artificial Intelligence*, vol. 37, no. 2, 2023, pp. 2366–2374.
- [47] Q. Liu, C. Chen, J. Qin, Q. Dou, and P.-A. Heng, “Feddg: Federated domain generalization on medical image segmentation via episodic learning in continuous frequency space,” in *Proceedings of the IEEE/CVF Conference on Computer Vision and Pattern Recognition*, 2021, pp. 1013–1023.
- [48] S. Li, C. Zhang, and X. He, “Shape-aware semi-supervised 3d semantic segmentation for medical images,” in *Medical Image Computing and Computer Assisted Intervention–MICCAI 2020: 23rd International Conference, Lima, Peru, October 4–8, 2020, Proceedings, Part I 23*. Springer, 2020, pp. 552–561.
- [49] X. Luo, J. Chen, T. Song, and G. Wang, “Semi-supervised medical image segmentation through dual-task consistency,” in *Proceedings of the AAAI conference on artificial intelligence*, vol. 35, no. 10, 2021, pp. 8801–8809.
- [50] K. Zhou, Y. Yang, Y. Qiao, and T. Xiang, “Domain adaptive ensemble learning,” *IEEE Transactions on Image Processing*, vol. 30, pp. 8008–8018, 2021.
- [51] Q. Liu, Q. Dou, and P.-A. Heng, “Shape-aware meta-learning for generalizing prostate mri segmentation to unseen domains,” in *Medical Image Computing and Computer Assisted Intervention–MICCAI 2020: 23rd International Conference, Lima, Peru, October 4–8, 2020, Proceedings, Part II 23*. Springer, 2020, pp. 475–485.
- [52] M. Segu, A. Tonioni, and F. Tombari, “Batch normalization embeddings for deep domain generalization,” *Pattern Recognition*, vol. 135, p. 109115, 2023.
- [53] S. Seo, Y. Suh, D. Kim, G. Kim, J. Han, and B. Han, “Learning to optimize domain specific normalization for domain generalization,” in *European Conference on Computer Vision*. Springer, 2020, pp. 68–83.
- [54] V. Olsson, W. Tranheden, J. Pinto, and L. Svensson, “Classmix: Segmentation-based data augmentation for semi-supervised learning,” in *Proceedings of the IEEE/CVF Winter Conference on Applications of Computer Vision*, 2021, pp. 1369–1378.
- [55] J. Zhang, Y. Zhang, and X. Xu, “Objectaug: object-level data augmentation for semantic image segmentation,” in *2021 International Joint Conference on Neural Networks (IJCNN)*. IEEE, 2021, pp. 1–8.